Deuteron elastic and inelastic scattering at intermediate energies from nuclei in the mass range $6 \leqslant A \leqslant 116$

A. Korff,[1] P. Haefner,[1] C. Bäumer,[1] A. M. van den Berg,[2] N. Blasi,[3] B. Davids,[2,*] D. De Frenne,[4] R. de Leo,[5] D. Frekers,[1] E.-W. Grewe,[1] M. N. Harakeh,[2] F. Hofmann,[6] M. Hunyadi,[2,†] E. Jacobs,[4] B. C. Junk,[1] A. Negret,[4,‡] P. von Neumann-Cosel,[6] L. Popescu,[4,‡] S. Rakers,[1] A. Richter,[6] and H. J. Wörtche[2]

[1]*Institut für Kernphysik, Westfälische Wilhelms-Universität Münster, Germany*
[2]*Kernfysisch Versneller Instituut, Rijksuniversiteit Groningen, The Netherlands*
[3]*Istituto Nazionale di Fisica Nucleare, Sezione di Milano, Italy*
[4]*Vakgroep Subatomaire en Stralingsfysica, Universiteit Gent, Belgium*
[5]*Dipartimento di Fisica, Università di Bari, Italy*
[6]*Institut für Kernphysik, Technische Universität Darmstadt, Germany*

(Received 28 May 2004; published 3 December 2004)

Angular distributions of differential cross sections for elastic and inelastic deuteron scattering from ^{6}Li, ^{16}O, ^{32}S, ^{50,51}V, and ^{70,72}Ge at an incident energy of 171 MeV and from ^{90}Zr and ^{116}Sn at an incident energy of 183 MeV are presented. Phenomenological optical-model parameters for elastic scattering are extracted from the data and compared to existing deuteron-nucleus global optical potentials.

DOI: 10.1103/PhysRevC.70.067601 PACS number(s): 25.45.De, 24.10.Ht, 24.10.Eq

Composite-particle scattering experiments at intermediate energies are now routinely being used as tools to probe nuclear strength functions. For instance, the $(d,{}^{2}\mathrm{He})$ reaction, whose study presently constitutes an active program at the AGOR facility (KVI, Groningen) [1–4], is a spin- and isospin-flip charge-exchange reaction, which probes the Gamow-Teller transition strength in the β^{+} direction. To extract this strength, a theoretical description of the distortion and absorption of the deuteron in the incident channel is mandatory and this is usually provided in terms of the optical model. This gave the motivation for an experiment to measure elastic and inelastic deuteron scattering from ^{6}Li, ^{16}O, ^{32}S, ^{50,51}V, and ^{70,72}Ge (at 171 MeV) and from ^{90}Zr and ^{116}Sn (at 183 MeV), as, for most of these isotopes, only few or no deuteron scattering data at intermediate energies are available. For instance, Nguyen *et al.* [5] performed deuteron scattering experiments on ^{16}O at 200, 400, and 700 MeV and van de Wiele *et al.* [6] determined optical-model parameters for 200 MeV deuteron scattering from ^{116}Sn. Note also that deuteron scattering data at similar energies within a mass range $12 \leqslant A \leqslant 58$ were presented in Refs. [7,8].

In the experiment, the deuteron beam was delivered by the superconducting cyclotron AGOR with an energy of 171 MeV and 183 MeV, respectively. Beam currents were measured with a Faraday cup and ranged from 0.1 nA to 2.2 nA depending on the spectrometer angle. Table I lists the target areal densities and enrichments for the investigated isotopes along with their chemical composition and type (self-supporting foil or pressed pellet). Areal densities of pressed targets were established by weighing the target and measuring the target area. Outgoing deuterons were momentum analyzed with the Big-Bite magnetic spectrometer [9] and detected with the focal-plane detection system of the ESN detector [10,11]. Measurements were performed at spectrometer angles ranging from 5° to 39° in steps of 2° and 3°. Additional measurements were made for ^{6}Li and ^{32}S at 48° and for ^{70,72}Ge at 42°. For some nuclei, the angular range between 10° and 14° was omitted due to the structural changes in the experimental setup necessary to measure in this angular range.

The analysis of the present study follows the one performed by Bäumer *et al.* [8] for ^{12}C, ^{24}Mg, and ^{58}Ni. Energy resolution was about 80–150 keV [full width at half maximum (FWHM)]. For all even-even isotopes angular distributions for inelastic scattering to the first $J^{\pi}=2^{+}$ states have been extracted and analyzed in terms of a deformed potential model. For ^{6}Li, a similar analysis was performed for the $J^{\pi}=3^{+}$ state at 2.186 MeV.

Two global optical potentials for deuteron scattering at intermediate energies are available. Daehnick *et al.* [12] have established a global optical potential that covers a target

TABLE I. Properties of the targets. P=pressed pellet, S=self-supporting foil.

Isotope	Areal density [mg/cm^2]	Enrichment [%]	Composition and type
^{6}Li	10.0	95.0	Li metallic (S)
^{16}O	11.4	nat. (99.8)	V_2O_5 (P)
^{32}S	8.6	nat. (95.0)	S powder (P)
^{50}V	11.4	55.4	V_2O_5 (P)
^{51}V	4.3	nat. (99.8)	V metallic (S)
^{70}Ge[a]	5.9/12.6	98.5	Ge met./GeO_2 (P)
^{72}Ge[a]	3.7/14.6	98.6	Ge metallic (P)
^{90}Zr	4.1	94.2	Zr metallic (S)
^{116}Sn	5.0	91.4	Sn metallic (S)

[a]Two different targets were used for the germanium isotopes.

*Present address: TRIUMF, Vancouver, B.C., Canada.
†Present address: ATOMKI, Debrecen, Hungary.
‡Permanent address: NIPNE, Bucharest, Romania.

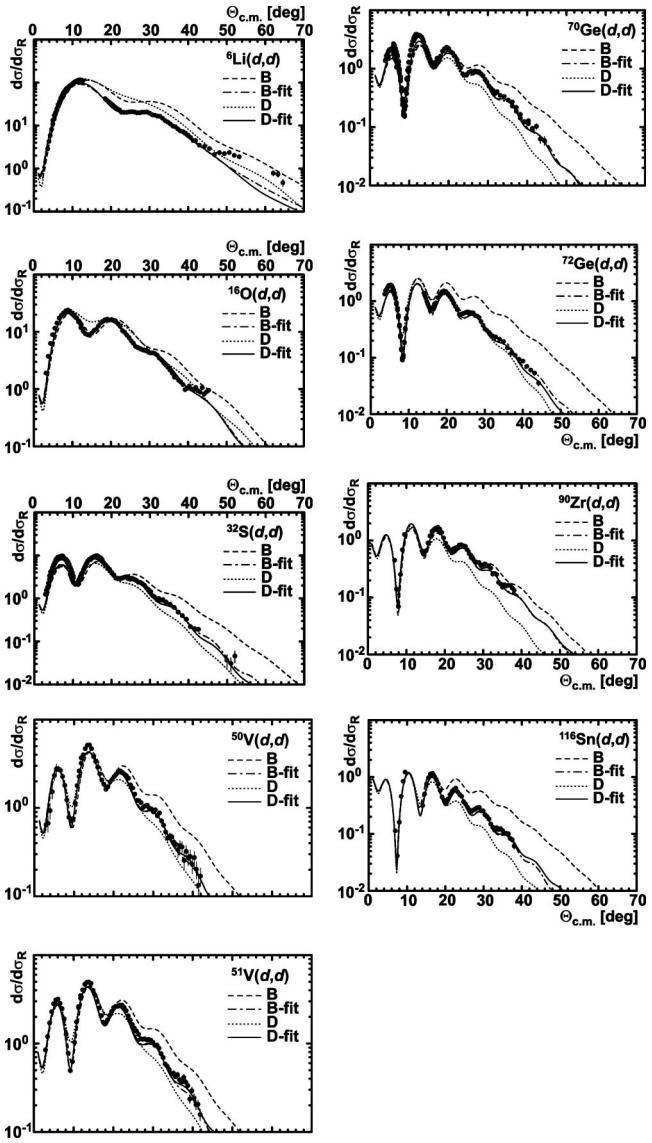

FIG. 1. Angular distributions for elastically scattered deuterons on ^{6}Li, ^{16}O, ^{32}S, ^{50,51}V, ^{70,72}Ge, ^{90}Zr, and ^{116}Sn as ratios of the differerential cross section to the Rutherford cross section. The curves are optical-model calculations discussed in the text.

mass range of $27 \leqslant A \leqslant 238$ and an energy range from 11.8 to 90 MeV. Another global parametrization has been given by Bojowald *et al.* [13], which covers a target mass range of $27 \leqslant A \leqslant 208$ at energies of 58.7 MeV and 85.0 MeV. We refer to Refs. [12,13] for the definition of the analytical expression describing the optical potential.

Starting with the extrapolated potentials of Bojowald *et al.* ("B") and Daehnick *et al.* ("D"), an improved set of parameters for each target, B-fit and D-fit, respectively, has been determined by fitting the relevant data to minimize the quantity $\chi^2 = \Sigma_{i=1}^{N} [(\sigma^{th} - \sigma_i^{expt})/\Delta\sigma_i^{expt}]^2$, where $\Delta\sigma_i^{expt}$ is the sum of the statistical and systematic errors for each data point i. The systematic error for self-supporting targets was estimated to be 10%, with the largest contribution coming from the uncertainty in the areal density of the target. Areal densities of pressed targets have a higher uncertainty of 15%. Targets containing impurities in the form of oxygen and carbon gave larger uncertainties at lower angles because of the necessity to resolve their overlapping elastic peaks through fitting. The cross sections for ^{50}V were derived from the measurement on a V_2O_2 target containing 45% ^{51}V and 55% ^{50}V and from the measurement on a natural metallic vanadium target (99.75% abundance ^{51}V). All figures in this work indicate only the statistical errors. Figure 1 displays the angular distributions for elastic scattering for all targets as a ratio to the Rutherford cross section along with the results of the calculations. The calculations were performed with the ECIS97 distorted-wave Born approximation (DWBA) code [14], which allows coupled-channels (CC) calculations. The

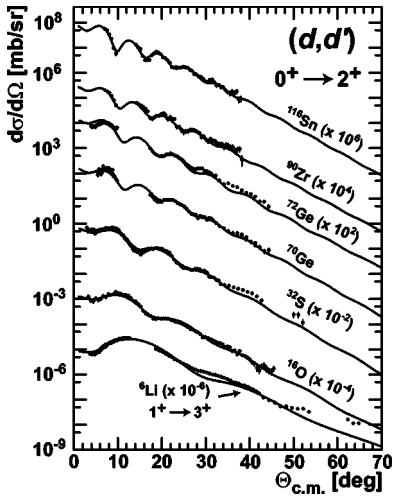

FIG. 2. Angular distributions for inelastic deuteron scattering to low-lying excited states in ^{6}Li, ^{16}O, ^{32}S, ^{70,72}Ge, ^{90}Zr, and ^{116}Sn. The solid curves represent the results of coupled-channels calculations with parameters given in Table II (BC-fit).

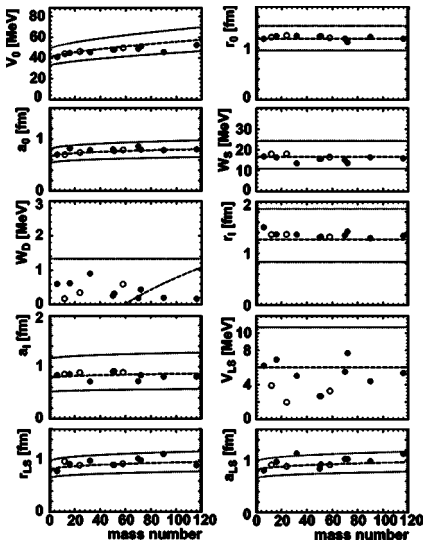

FIG. 3. The optical-model parameters of B-fit plotted against the mass number of their respective nuclei. The results of Ref. [8] are shown as open circles. The extrapolation of the Bojowald global potential to $E_d = 171$ MeV is indicated as dashed line. The dotted lines represent the boundaries of parameter variation (except for ^{32}S).

TABLE II. Optical-potential parameters derived from our best fit to the experimental data, volume integrals for the real, imaginary, and spin-orbit parts of the optical potential, and the total reaction cross section σ_R which is calculated with the ECIS code. The last column shows the relative χ^2 of the calculation. Fits that used the potential of Daehnick *et al.* or Bojowald *et al.* as starting points are denoted with D-fit and B-fit, respectively. The corresponding CC calculations, which were compared to the elastic and inelastic data sets, are denoted by DC-fit and BC-fit.

	Target	V_R [MeV]	r_0 [fm]	a_0 [fm]	W_S [MeV]	W_D [MeV]	r_I [fm]	a_I [fm]	V_{LS} [MeV]	r_{LS} [fm]	a_{LS} [fm]	$J_R/2A$	$J_I/2A$ [MeV fm^3]	$J_{LS}/2A$	σ_R [mb]	χ^2/N
D-fit	^{6}Li	42.07	1.214	0.721	15.68	0.74	1.445	0.870	2.21	1.051	0.679	325	233	9.0	479	2.37
DC-fit	^{6}Li	42.07	1.214	0.721	17.40	0.82	1.381	0.841	2.21	1.051	0.679	325	228	9.0	471	6.30
B-fit	^{6}Li	40.91	1.178	0.701	16.81	0.60	1.504	0.840	6.20	0.789	0.810	290	253	20	505	2.23
BC-fit	^{6}Li	40.91	1.178	0.701	18.02	0.57	1.348	0.985	6.20	0.789	0.810	290	265	20	546	3.59
D-fit	^{16}O	45.68	1.229	0.870	16.22	0.93	1.446	0.686	4.86	1.032	0.788	316	153	10	634	0.47
DC-fit	^{16}O	45.68	1.229	0.870	18.02	0.94	1.402	0.723	4.86	1.032	0.788	316	162	10	658	1.01
B-fit	^{16}O	44.78	1.233	0.823	16.39	0.62	1.368	0.861	6.91	0.925	0.972	298	154	13	680	0.58
BC-fit	^{16}O	44.78	1.233	0.823	18.21	0.69	1.311	0.894	6.91	0.925	0.972	298	161	13	702	0.72
D-fit	^{32}S	52.06	1.188	0.807	13.50	0.23	1.424	0.718	2.51	1.165	0.902	266	105	3.7	844	1.67
DC-fit	^{32}S	52.06	1.188	0.807	15.00	0.25	1.377	0.777	2.51	1.165	0.902	266	111	3.7	884	1.65
B-fit	^{32}S	45.43	1.235	0.786	13.53	0.90	1.363	0.717	5.03	0.987	1.136	250	102	6.3	821	1.66
BC-fit	^{32}S	45.43	1.235	0.786	15.02	0.90	1.312	0.792	5.03	0.987	1.136	250	107	6.3	867	1.66
D-fit	^{50}V	49.00	1.218	0.848	15.98	1.03	1.360	0.696	3.39	1.082	0.762	251	110	3.4	1123	0.47
B-fit	^{50}V	48.08	1.224	0.802	15.66	0.26	1.309	0.910	2.68	0.913	0.843	242	103	2.3	1173	0.52
D-fit	^{51}V	49.00	1.225	0.819	15.99	1.04	1.373	0.701	3.42	1.113	0.754	249	113	3.5	1159	0.37
B-fit	^{51}V	48.08	1.233	0.770	15.66	0.32	1.321	0.916	2.67	0.909	0.927	242	106	2.2	1215	0.38
D-fit	^{70}Ge	47.28	1.202	0.810	14.79	0.40	1.310	0.795	3.64	1.282	0.949	217	88	3.5	1289	1.39
DC-fit	^{70}Ge	47.28	1.202	0.810	15.88	0.37	1.309	0.754	3.64	1.282	0.949	217	92	3.5	1301	1.29
B-fit	^{70}Ge	48.85	1.182	0.858	15.04	0.19	1.348	0.723	5.51	1.030	1.030	221	92	4.2	1282	1.92
BC-fit	^{70}Ge	48.85	1.182	0.858	16.68	0.19	1.299	0.788	5.51	1.030	1.030	221	95	4.2	1320	1.64
D-fit	^{72}Ge	53.97	1.095	0.849	15.52	0.40	1.324	0.948	6.32	1.057	1.025	199	102	4.9	1493	0.43
DC-fit	^{72}Ge	53.97	1.095	0.849	17.22	0.44	1.273	0.963	6.32	1.057	1.025	199	103	4.9	1490	1.12
B-fit	^{72}Ge	51.28	1.115	0.799	13.65	0.44	1.421	0.839	7.67	0.998	1.029	193	103	5.6	1495	0.59
BC-fit	^{72}Ge	51.28	1.115	0.799	15.16	0.45	1.355	0.905	7.67	0.998	1.029	193	104	5.6	1511	1.52
D-fit	^{90}Zr	47.28	1.212	0.809	14.50	0.58	1.320	0.744	2.94	1.145	0.791	215	85	2.1	1456	1.14
DC-fit	^{90}Zr	47.28	1.212	0.809	15.92	0.58	1.279	0.823	2.94	1.145	0.791	215	89	2.1	1497	1.18
B-fit	^{90}Zr	45.72	1.215	0.786	16.36	0.20	1.294	0.809	4.41	1.118	0.986	207	90	3.1	1489	0.87
BC-fit	^{90}Zr	45.72	1.215	0.786	17.19	0.50	1.261	0.839	4.41	1.118	0.986	207	92	3.1	1506	0.95
D-fit	^{116}Sn	52.99	1.186	0.802	15.46	0.14	1.355	0.807	2.79	1.052	0.784	221	94	1.6	1822	0.89
DC-fit	^{116}Sn	52.99	1.186	0.802	16.38	0.13	1.332	0.854	2.79	1.052	0.784	221	96	1.6	1857	1.08
B-fit	^{116}Sn	52.62	1.179	0.802	15.88	0.17	1.339	0.814	5.36	0.901	1.130	215	94	2.6	1808	0.67
BC-fit	^{116}Sn	52.62	1.179	0.802	17.02	0.18	1.313	0.858	5.36	0.901	1.130	215	96	2.6	1839	1.00

fitting procedure for each isotope consisted of two stages, and each stage was subdivided into two steps. In the first step, a Monte Carlo search was carried out and the parameter set with the smallest χ^2 was selected. In the second step, each parameter of this set was varied in the direction of smaller χ^2, until a minimum was found. In each stage, the parameters were allowed to vary by about 20% from the starting potential, except for two parameters which were assigned *a priori* value ranges. These were the spin-orbit potential depth V_{LS}, where a 20% variation seemed insufficient to find good fits, and the surface absorption potential depth W_D, as it gives an unphysical value (<0 MeV) in the case of the Bojowald starting potential. In the first stage, a combined fit including the elastic and inelastic data sets was performed in a CC framework to fix the real potential parameters, resulting in the parameter sets BC-fit and DC-fit. We assumed in the CC calculation a rotational model for ^{6}Li and a vibrational model for ^{16}O [15], ^{32}S [16], ^{70,72}Ge [17], ^{90}Zr [18], and ^{116}Sn [19]. The coupling strengths were fitted to the data, using the values of the references cited above as starting points whenever possible and allowing for a 20% variation. The exception was ^{6}Li, where no literature values could be found and, thus, an arbitrary starting point was chosen which was allowed to vary from -1.0 to 1.0. The β_2 parameters

determined in these calculations are ±0.89 (^{6}Li), 0.22 (^{16}O), 0.24 (^{32}S), 0.22 (^{70}Ge), 0.24 (^{72}Ge), 0.08 (^{90}Zr), and 0.11 (^{116}Sn).

Figure 2 shows the angular distributions for the inelastic transition to the first excited state together with the results of the CC calculations using the parameters given in Table II (BC-fit). In the second stage, only the elastic data sets were fitted, while keeping the real potential parameters fixed to the values derived from the CC fit and allowing only the imaginary potential parameters to vary. The resulting parameter sets are labeled B-fit and D-fit, respectively. All potential parameters obtained in this way are presented in Table II.

Obviously, the B potential overestimates the cross section at larger angles due to its large spin-orbit potential depth of 6 MeV, while the D potential underestimates the cross section. This difference increases with larger mass numbers. Our best fit generally lies between these two extremes, with the exception of the lightest nuclei ^{6}Li and ^{16}O. The B potential describes the magnitude of the first minimum of the diffraction pattern well, though it is slightly out of phase. The D potential fails to properly represent the structure of the distributions, which is especially obvious again in the case of the two lightest nuclei (^{6}Li and ^{16}O), but is visible in all other nuclei as well. Especially the depth of the first minimum is not well reproduced by the D potential, though this effect decreases with increasing mass number. One may note that a description of scattering on light nuclei ($A \lesssim 24$) in terms of the phenomenological optical model is not well defined [20] and fully microscopic calculations might be preferred. Depending on the starting potential, the best fits yield dissimilar parameter sets, but the quality is in both cases acceptable. In general, the optical-model calculations with optimized parameters still tend to underestimate the magnitude of some maxima, but at larger angles the agreement with the data is improved. For most nuclei, the volume integrals of the imaginary and real potential parts are increased in our best fits compared to the starting potentials. The spin-orbit volume integrals tend to show a large scatter, but this is mainly a result of the different starting values of the global potentials. A cross-check can be performed for ^{16}O by comparing the vector analyzing power A_y calculated with the best-fit parameter sets to those measured at 200 MeV [5]. It is found that the calculations agree in magnitude with the measured data, though the diffraction pattern is not well reproduced at angles larger than 25°. Graphs of the optical-model parameters from the parameter set B-fit as a function of the mass number are depicted in Fig. 3 together with the extrapolations of the global potential of Bojowald *et al.* Obviously, the only parameters to significantly deviate from the global potential are those that were given larger ranges during the fitting procedure—namely, W_D and V_{LS}.

To summarize, we presented deuteron scattering data for ^{6}Li, ^{16}O, ^{32}S, ^{50,51}V, and ^{70,72}Ge at an incident energy of 171 MeV and for ^{90}Zr and ^{116}Sn at 183 MeV. The experimental data have been compared to optical-model calculations based on extrapolated global potentials and improved parameter sets have been deduced.

We would like to thank S. Brandenburg and the accelerator staff at the KVI. We thank H. Baumeister (IKP Münster) for the production of the targets. This work was performed with support from the Land Nordrhein-Westfalen and from the EU under Contract No. TMR-LSF HPRI-1999-CT-00109. It was further performed as part of the research program of the Stichting FOM with financial support from the Nederlandse Organisatie voor Wetenschappelijk Onderzoek and as part of the research program of the Fund for Scientific Research-Flandres. This work has further been supported by the Deutsche Forschungsgemeinschaft DFG under Contract No. SFB 634.d.

[1] C. Bäumer *et al.*, Phys. Rev. C **68**, 031303(R) (2003).
[2] D. Frekers, Nucl. Phys. **A731**, 76 (2004).
[3] S. Rakers *et al.*, Phys. Rev. C **65**, 044323 (2002).
[4] E.-W. Grewe *et al.*, Phys. Rev. C **69**, 064325 (2004).
[5] Nguyen Van Sen *et al.*, Nucl. Phys. **A464**, 717 (1987).
[6] J. van de Wiele *et al.*, Phys. Rev. C **50**, 2935 (1994).
[7] Nguyen Van Sen *et al.*, Phys. Lett. **156**, 185 (1985).
[8] C. Bäumer *et al.*, Phys. Rev. C **63**, 037601 (2001).
[9] A. M. van den Berg, Nucl. Instrum. Methods Phys. Res. B **99**, 637 (1995).
[10] V. M. Hannen *et al.*, Nucl. Instrum. Methods Phys. Res. A **500**, 68 (2003).
[11] H. J. Wörtche, Nucl. Phys. **A687**, 321 (2001).
[12] W. W. Daehnick, J. D. Childs, and Z. Vrcelj, Phys. Rev. C **21**, 2253 (1980).
[13] J. Bojowald, H. Machner, H. Nann, W. Oelert, M. Rogge, and P. Turek, Phys. Rev. C **38**, 1153 (1988).
[14] J. Raynal, "Notes on ECIS94," Note No. CEA-N-2772, 1994, ECIS97 (unpublished).
[15] E. Fabrici, S. Micheletti, M. Pignanelli, F. G. Resmini, R. De Leo, G. D'Erasmo, and A. Pantaleo, Phys. Rev. C **21**, 844 (1980).
[16] M. Herman, EMPIRE-II, International Atomic Energy Agency, Vienna, Austria, 2002.
[17] S. Raman, C. W. Nestor, S. Kahane, and K. H. Bhatt, At. Data Nucl. Data Tables **42**, 1 (1989).
[18] L. Kurth, B. C. Clark, E. D. Cooper, S. Hama, S. Shim, R. L. Mercer, L. Ray, and G. W. Hoffmann, Phys. Rev. C **49**, 2086 (1994).
[19] B. Bonin *et al.*, Nucl. Phys. **A445**, 381 (1985).
[20] A. J. Koning and J. P. Delaroche, Nucl. Phys. **A713**, 231 (2003).